Reanalysis of a municipal landfill slope failure near Cincinnati, Ohio, USA

Ashok K. Chugh, Timothy D. Stark, and Kees A. DeJong

Abstract: The March 1996 slope failure in a municipal solid waste landfill near Cincinnati, Ohio, USA, is reanalyzed using continuum-mechanics-based procedures implemented in the computer programs FLAC and FLAC3D. A failure mechanism, based on the field observations of the failure, is used for the analyses. The failure mechanism is also implemented in a limit-equilibrium-based slope stability analysis computer program, SSTAB2, to simulate the observed translational character of the failure. The reanalysis results (failure surface, factor-of-safety (FoS), and displacement) from the continuum models are in general agreement with the field data. The FoS values from SSTAB2, FLAC, and FLAC3D range in the expected order. Overall, the reanalysis results supplement previously reported failure analyses. This paper serves two functions: (1) it documents the results of reanalysis using a different (from the previously published) failure mechanism hypothesis for the 1996 landfill slope failure near Cincinnati, Ohio; and (2) it demonstrates the use of 2-D and 3-D continuum models to study: (*i*) onset of instability; (*ii*) failure surface geometry and location; and (*iii*) displacements associated with slope failures.

Key words: municipal landfill, slope failure, numerical analysis, limit equilibrium, continuum mechanics, displacement.

Résumé : La rupture d'un talus en mars 1996 dans un site municipal d'enfouissement de solides près de Cincinnati, Ohio, E.U., est réanalysée au moyen de procédures basées sur la mécanique des milieux continus mises en application dans les programmes d'ordinateur FLAC et FLAC3D. Le mécanisme de rupture, basé sur des observations sur le terrain, est utilisé pour les analyses. Le mécanisme de rupture est aussi utilisé dans un programme d'ordinateur pour une analyse de stabilité de talus basée sur l'équilibre limite SSTAB2 pour simuler le caractère de translation de la rupture observée. Les résultats de la réanalyse (surface de rupture, coefficient de sécurité « FoS », déplacement) issus des modèles de continuum sont généralement en concordance avec les données de terrain. Les valeurs de FoS obtenues par les programmes SSTAB2, FLAC et FLAC3D varient dans l'ordre prévu. En somme, les résultats de réanalyse apportent un complément aux analyses de rupture rapportées antérieurement. Cet article a deux buts : (1) documenter les résultats de réanalyse au moyen d'une hypothèse de mécanisme de rupture différente de celles publiées antérieurement pour la rupture du talus le site d'enfouissement de 1996 près de Cincinnati, Ohio; et (2) démontrer l'utilisation de modèles de continuum 2-D et 3-D pour étudier : (*i*) le déclenchement de l'instabilité; (*ii*) la géométrie et la localisation de la surface de rupture; et (*iii*) les déplacements associés aux ruptures de pente.

Mots-clés : enfouissement municipal, rupture de pente, analyse numérique, équilibre limite, mécanique des milieux continus, déplacements.

[Traduit par la Rédaction]

Introduction

On 9 March 1996, a large slope failure occurred in a municipal solid waste (MSW) landfill approximately 15 km northwest of Cincinnati, Ohio, USA. Figure 1*a* shows the location map of the MSW site, and Fig. 1*b* shows an aerial view of the failure with annotations of significant items including the preslide excavation for an access road at the toe of the landfill. This failure was described and analyzed by Eid et al. (2000) and Stark et al. (2000) using a limit-equilibrium-based procedure implemented in the computer program CLARA (Hungr 1988). In those studies (as in other slope failures), there were uncertainties with regard to leachate level, mobilized shear strength in the brown native soil underlying the waste, and the effects of excavation and blasting near the toe of the landfill as a trigger of the wasteslide (Kavazanjian et al. 2001). Stark et al. (2000) recommended a deformation analysis of the failure to gain a better and (or) improved understanding of the role of some of these uncertainties in the failure and the shear strength mobilized in the brown native soil. The reanalysis presented herein supplements this earlier work on the slope failure.

The objectives of this paper are to present: (*i*) a working hypothesis for the failure mechanism based on field observations; (*ii*) an implementation of the hypothesis in a limit-equilibrium-based slope stability analysis procedure SSTAB2 (Chugh 1992) to estimate the pore-pressure conditions (leachate level) at the onset of the slope failure using

Received 27 July 2005. Accepted 14 August 2006. Published on the NRC Research Press Web site at http://cgj.nrc.ca on 10 February 2007. Reposted on the Web site with corrections on 12 February 2007.

A.K. Chugh.[1] U.S. Bureau of Reclamation, P.O. Box 25007, Denver, CO 80225–0007, USA.
T.D. Stark. University of Illinois, MC-250, Urbana, IL 61801–2352, USA.
K.A. DeJong. University of Cincinnati, P.O. Box 0013, Cincinnati, OH 45221–0013, USA.

[1]Corresponding author (e-mail: achugh@do.usbr.gov).

 doi:10.1139/T06-089

Fig. 1. Landfill site (reproduced with permission of ASCE).

(a) Location map

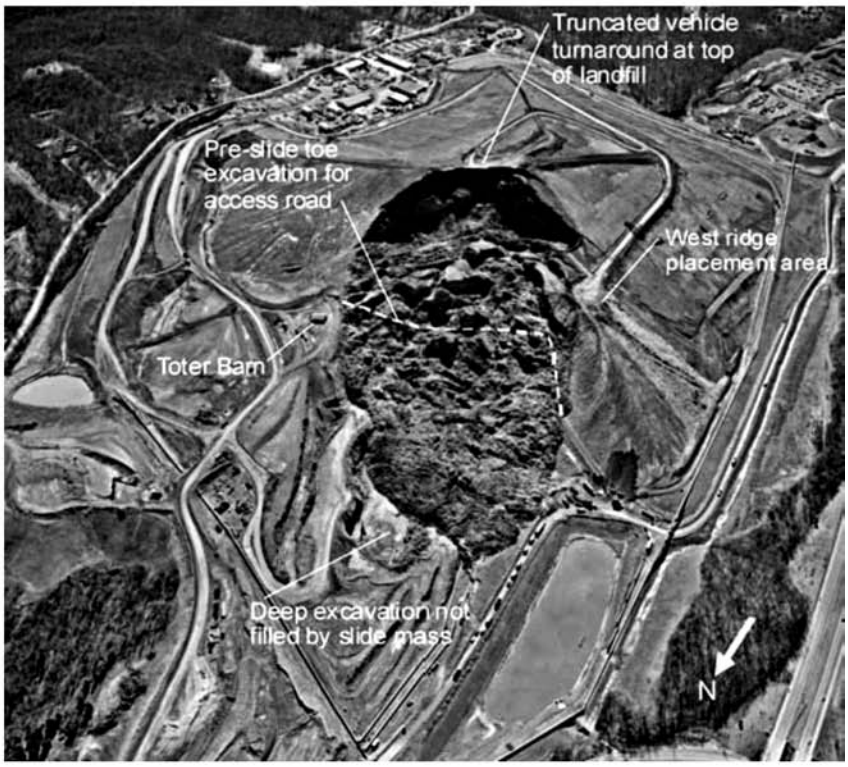

(b) Aerial view of the failure (Stark et al. 2000)

data in Eid et al. (2000); and for continuum-mechanics-based analyses: (*iii*) results of two-dimensional (2-D) static slope stability and deformation analyses using the procedure implemented in the computer program FLAC (Itasca 2000); and (*iv*) results of three-dimensional (3-D) static slope stability analysis using the procedure implemented in the computer program FLAC3D (Itasca 2002). For ease of presentation, 2-D cross-sections are assumed to lie in the x–z plane and the x,y,z coordinate system used herein follows the right hand rule.

This paper serves two functions: (1) it documents the results of the reanalysis using a different (from the previously published) failure mechanism hypothesis for the 1996 landfill slope failure near Cincinnati, Ohio; and (2) it demonstrates the use of 2-D and 3-D continuum models to study: (*i*) the onset of instability; (*ii*) the failure surface geometry and location; and (*iii*) the displacements associated with slope failures.

The project data (contour maps of the landfill site) are in Imperial units and they are presented herein as such; the remainder of the presentation of this paper is in SI units.

Landfill site description and field conditions

Descriptions of the areal geology were presented by Baum and Johnson (1996) and the local geology by Eid et al. (2000). The subsurface conditions under the landfill consist of a 2–5 m thick layer of brown native soil (NS) overlying a slightly dipping (1–2 m/km) bedrock formation of shale and interbedded limestone. The landfill site has experienced three or possibly four continental ice advances.

In the 1940s, MSW was deposited at the site over the brown native soil; at that time no liner system was required prior to waste placement.

Figure 2 shows the site contour maps of the landfill site: (*i*) prior to commencement of the landfill in the 1940s; (*ii*) prior to the wasteslide in 1996 including the deep excavation below the toe of the landfill (for lateral expansion of the facility and increased air space); and (*iii*) after the landfill failure.

The leachate conditions prior to the wasteslide are not known. From field observations and boring logs after the wasteslide, Stark et al. (2000) provided an estimate of the leachate level that could have existed prior to the failure.

From large-scale laboratory and field tests results and back-analysis of failed waste slopes, Eid et al. (2000) recommended the following material properties. For the MSW: density (ρ) equal to 1040 kg/m^3, friction angle (ϕ) equal to 35°, and cohesion (c) equal to 4.0×10^4 Pa; and for the brown native soil (NS): ρ = 2010 kg/m^3, ϕ = 23° (fully softened) and 12° (residual), and c = 0. Figure 3 shows a summary of the test data results.

The main cause of wasteslide is attributed to mobilization of a post-peak shear strength in the NS, which has been described as colluvium (Stark et al. 2000).

Summary of field observations

The following details of the wasteslide, taken from Stark et al. (2000), are considered significant in the development

Fig. 2. Contour maps of the landfill site with footprint of failure superimposed (contour interval: 20 ft; 1 ft = 0.30 m).

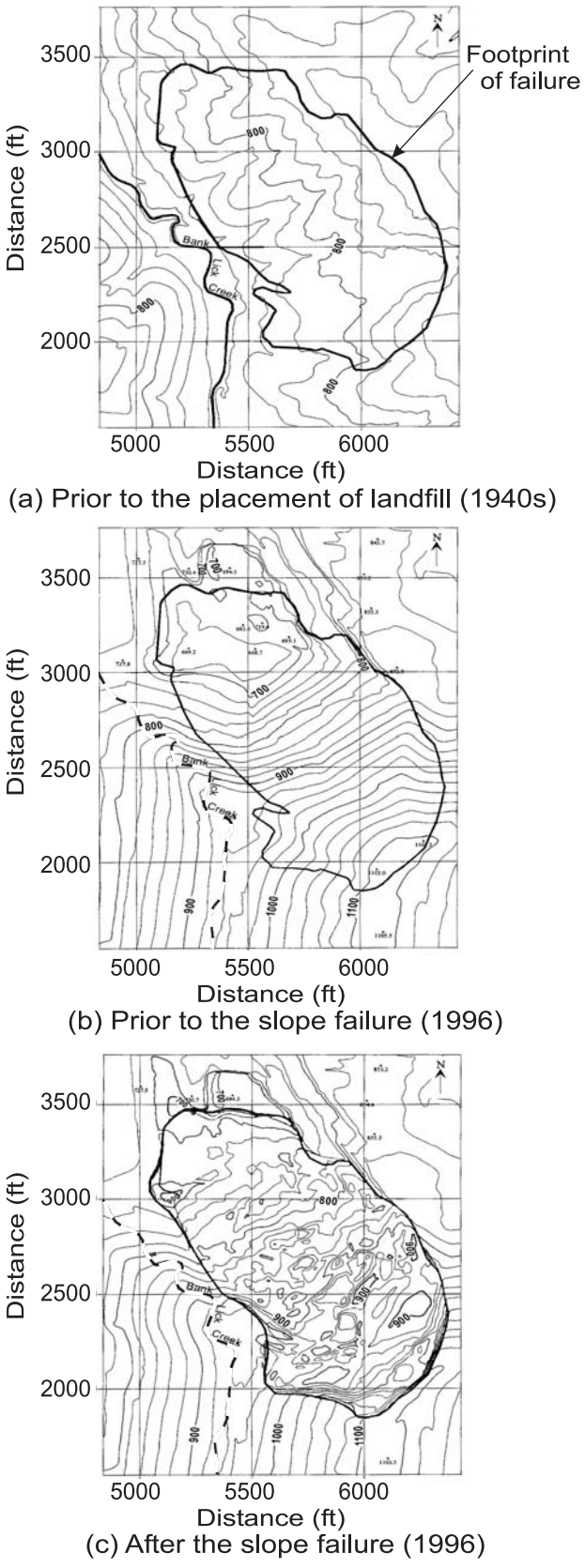

Fig. 3. Laboratory test data on the brown native soil (NS) and gray shale at the landfill site (Eid et al. 2000, reproduced with permission of ASCE).

(a) Index properties (%)

Sample	LL	PL	CF
■ Gray shale	36	20	44
▲ Brown native soil (NS)	63	27	53
● Brown native soil (NS)	69	28	55

LL - Liquid limit; PL - Plastic limit;
CF - Clay fraction

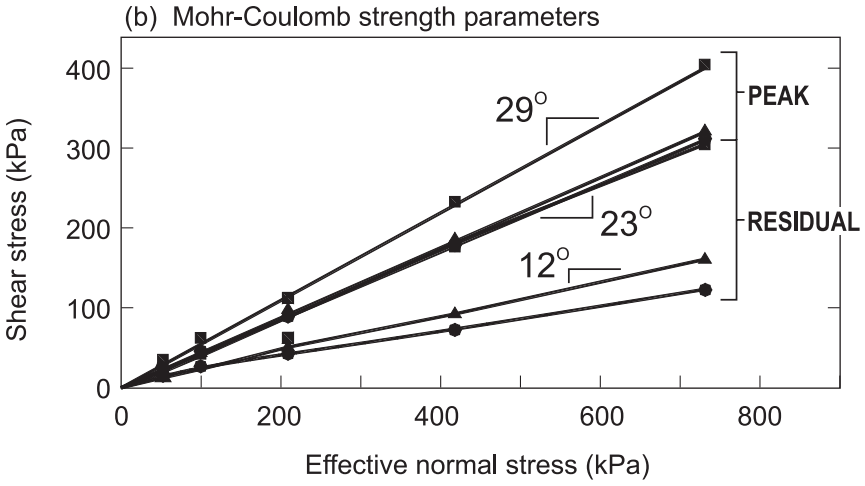

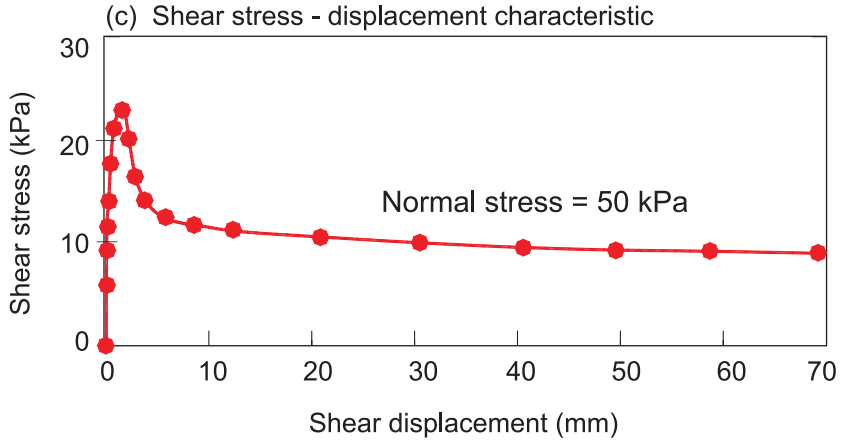

of the working hypothesis for the failure mechanism used herein:

(1) Prior to the occurrence of the wasteslide — (*i*) Continual collection of leachate and surface water contaminated by the leachate occurred in the deep excavation at the toe of the landfill; (*ii*) Bedrock seepage broke through the partially completed compacted clay liner on the 3*H*:1*V* slope into the deep excavation; (*iii*) Springtime rainfall in the area had commenced; (*iv*) The shale bedrock at the site was jointed; and (*v*) Tension cracks appeared and reappeared in the same location(s) at the crest of the waste slope for 5 days prior to the occurrence of the wasteslide; landfill personnel covered these cracks (believing them to be settlement induced) daily with soil to reduce infiltration.

(2) On the day of the wasteslide — (*i*) The tension cracks appearing at the crest of the waste slope extended down the east side of the slope and steam emanated from the

cracks; (*ii*) A graben started forming near the top of the landfill corresponding to the vicinity of the tension cracks that had been appearing and reappearing prior to the occurrence of the wasteslide; (*iii*) The cracks appearing on the crest and the east side of the waste slope extended to the west side of the slope; (*iv*) The waste on the eastern side of the slope, i.e., the external slope, moved first and slowly toward the deep excavation; (*v*) The eastern movement involved the slope toe moving across the access road towards the deep excavation and eventually into the deep excavation; and finally (*vi*) A large slide block accelerated toward the deep excavation and completed the wasteslide within a few minutes.

(3) After the wasteslide — (*i*) Some sloughing at the top of the landfill and the final wasteslide scarp occurred with the final scarp being 30–60 m high and nearly vertical; (*ii*) A leachate pool developed after about 3 months at the base of the graben—the leachate pool elevation was approximately 268.4 m; and (*iii*) The toe of the existing slope moved approximately 245–275 m to the northern wall of the deep excavation.

(4) From field observations and subsurface investigations— (*i*) The translational failure occurred through the NS underlying the MSW; (*ii*) The failure surface passed through the solid waste at a steep inclination to the NS from the tension cracks observed at the top of the slope; (*iii*) The failure surface daylighted at the vertical excavation at the slope toe that had exposed the MSW and the NS; (*iv*) The NS was soft and saturated prior to the wasteslide (based on borings after the slide); and (*v*) The MSW was fairly dry prior to the wasteslide (based on old newspapers recovered in borings after the slide being easily readable).

(5) From laboratory tests — The transition from peak to residual shear strength of the NS occurred in a brittle fashion, Fig. 3*c*.

Working hypothesis for the failure mechanism

Using Brooker and Peck (1993) as a guide, the following working hypothesis for the failure mechanism of the landfill slide was developed and is shown in Fig. 4.

Because the observed failure surface passed through the landfill at a steep inclination (almost vertical), there is little (or no) active wedge pushing on the middle (neutral) wedge of the slide mass. Also absent from the wasteslide is the presence of a passive wedge. Thus the traditional 3-part slide-mass model of a slope composed of an active, a neutral, and a passive wedge does not fit this wasteslide.

The state of stress in the landfill is due to the gravitational effects in the vertical direction and lateral confinements in the horizontal directions. The lateral stresses in the landfill correspond to the at-rest earth pressure conditions (first time failure), Fig. 4*a*. The shear resistance of the brown native soil could be less than in a first time failure (fully softened shear strength) because of prior (before the 1940s) shear movement during the development of the colluvial deposit. In addition, the NS layer has been compressed in the vertical

Fig. 4. Failure mechanism hypothesis: K_0, at-rest lateral pressure coefficient; γ, unit weight (adapted from Brooker and Peck 1993).

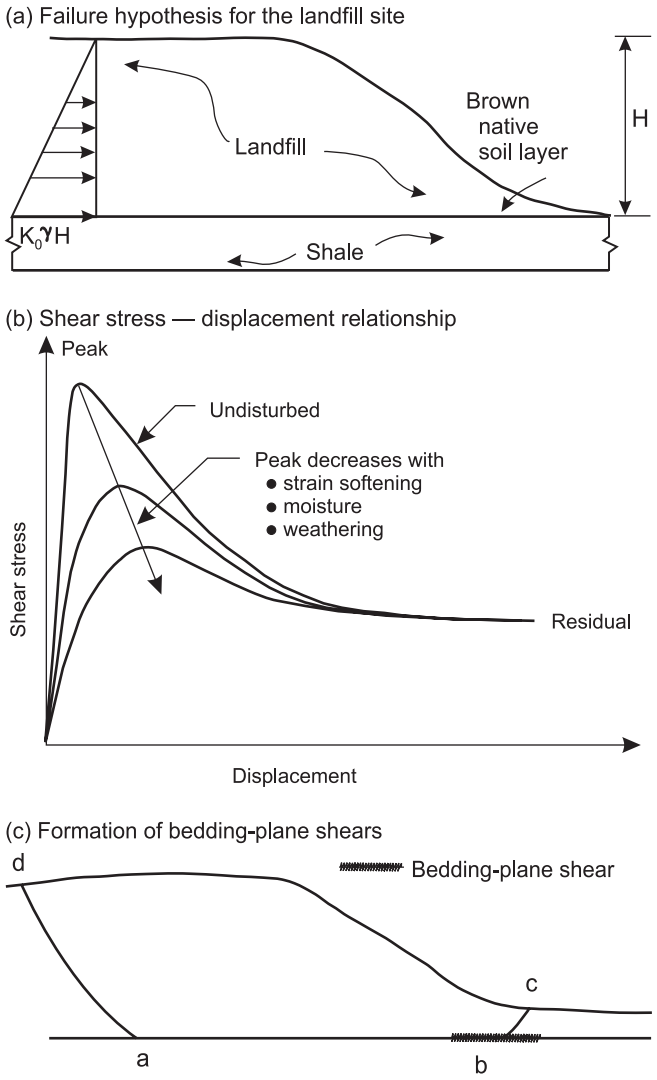

direction by the weight of the MSW, and due to preslide confinements in the lateral directions (that prevented lateral spreading) must have induced lateral stresses. The essentially vertical excavation (for the access road) along the toe of the landfill reduced the lateral confining stresses acting on the landfill and the brown native soil to zero at this location. Because a noncohesive soil adjacent to an unsupported vertical cut can not be stable, some lateral movement of the brown native soil near the toe is inevitable to attain a stable configuration. As illustrated in Fig. 4*c*, an overall equilibrium could have been maintained with sufficient shearing resistance along the inclined (1–2 m/km slope) and relatively thin brown native soil layer represented in the figure by a contact plane between the MSW and underlying bedrock. If the shearing resistance of the brown native soil is exceeded along all or part of the contact plane, slip or shear displacement occurs, and the shearing strength is reduced from the initial value to a smaller value, as shown in Fig. 4*b*. If the shear displacement is large enough, the shear strength can be

Fig. 5. Footprint of failure and location of planar cross-sections (contour interval: 10 ft (MSW), 50 ft (bedrock); 1 ft = 0.30 m) (adapted from Stark and Eid 1998, reproduced with permission of ASCE).

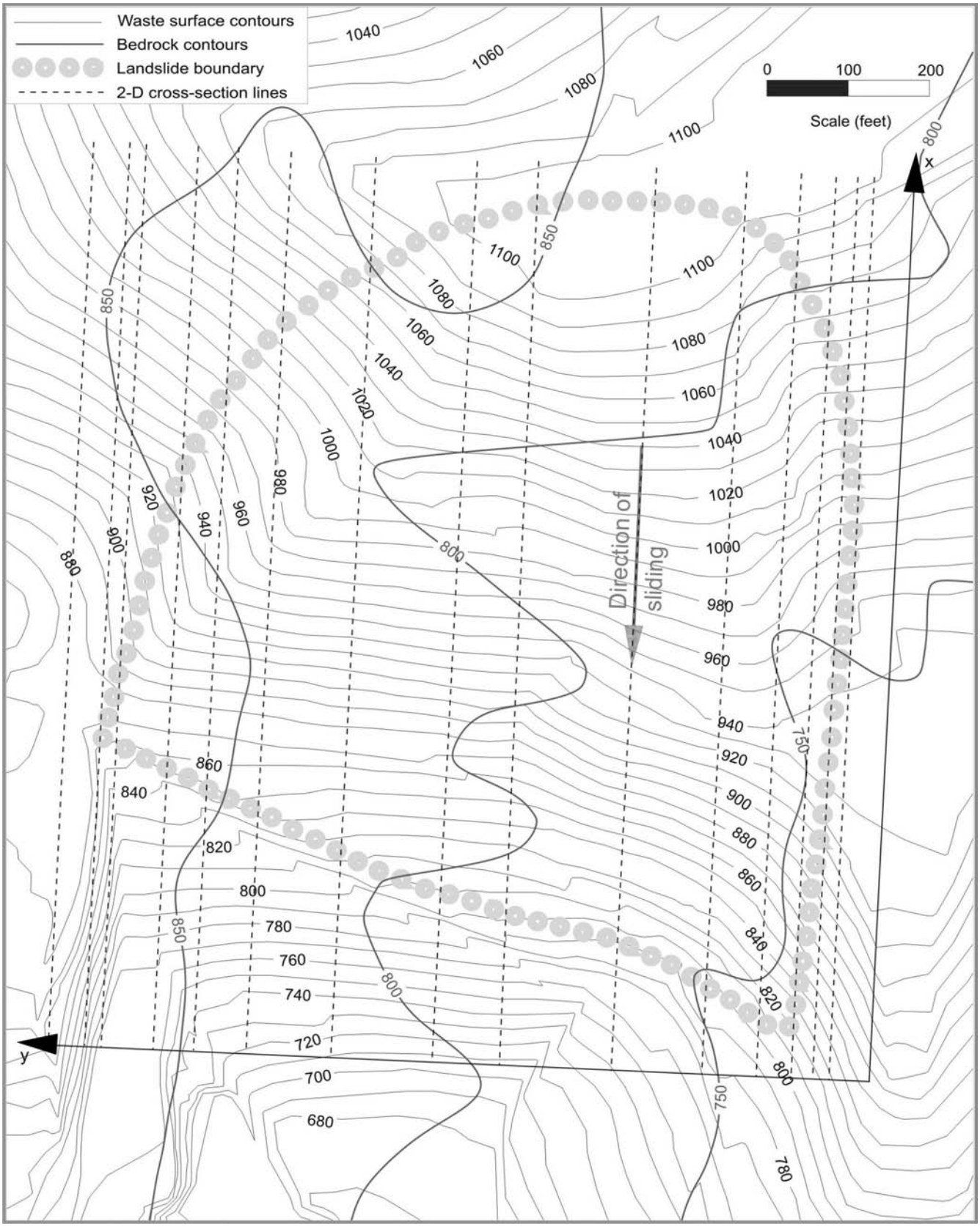

reduced to the residual value, Figs. 4*b* and 3*c*. Thus, the proposed failure mechanism for the wasteslide is one of progressive failure, Fig. 4*c*.

Numerical reanalysis

Figure 5 shows a plan view of the wasteslide and the location of the 16 cross-sections used in the reanalyses; 10 of these cross-sections include the landfill slide mass and the other 6 are used to enforce the lateral boundary conditions in a 3-D model of the wasteslide. Figure 6 shows the cross-sectional views along the 16 locations marked on Fig. 5. For factor of safety (FoS) calculations, planar analyses for the 10 (participating) cross-sections were performed using the 2-D limit-equilibrium-based solution procedure implemented in the computer program SSTAB2, and the continuum-mechanics-based solution procedure implemented in the computer program FLAC. The 3-D continuum FoS model used all 16 cross-sections and the analysis was performed using the solution procedure implemented in the computer program FLAC3D. Deformation analyses of the wasteslide were made using the 10 (participating) planar cross-sections shown in Fig. 6 and the computer program FLAC. The NS layer was assumed to be 5 m thick in these numerical models. Table 1 shows the material properties values used for stability and deformation analyses; the property values for the MSW and NS are taken from Stark et al. (2000); the shale and interface (between MSW and NS) property values are assumed.

2-D limit-equilibrium analyses

SSTAB2 implements Spencer's (1967) limit-equilibrium procedure for planar (2-D) slope stability analyses. The procedure satisfies all equations of static equilibrium and thus provides a reliable estimate of FoS (Duncan and Wright 2005). The results of the analysis are in terms of FoS and the associated interslice force inclination angle, δ. The objective of these analyses was to estimate the leachate level required to cause the slope to become unstable, i.e., FoS $\approx$ 1. For each of the 10 participating cross-sections, the leachate level estimated from field observations was imposed on the MSW in the form of a piezometric line, and the value of pore-pressure ratio, r_u, (pore pressure/overburden vertical stress) for the NS was determined for FoS $\approx$ 1. Field estimated failure surfaces were used in these calculations. The at-rest earth pressure was calculated using the relation $\sigma_{xx} = K_0\, \rho_{MSW} g h$, where K_0 is the at-rest lateral pressure coefficient assigned an assumed value of 0.43. This value of K_0 is well within the range of values (0.2 to 1.0) measured and reported in the literature for MSW (Kavazanjian 2006). The at-rest earth pressure was applied through the full depth of the MSW via a tension crack (vertical) filled with liquid of adjusted density ρ = 447.2 kg/m^3, and the height of the piezometric line (representing the leachate level) was adjusted by multiplying the estimated phreatic line data by $\rho_{water}/K_0\rho_{MSW} = 2.24$.

Figure 7*a* shows a typical SSTAB2 model of the 10 cross-sections that participated in the 1996 wasteslide. This cross-section is located at y = 138 m (Figs. 5 and 6). For each of the 10 cross-sections analyzed, the value of r_u, and (FoS, δ) achieved are given in Table 2. The equivalent phreatic line that corresponds to the r_u value in the NS plots differently (higher and (or) lower) than that estimated from field observation and used for the MSW in this paper. For the cross-section at y = 138 m, plots of the calculated equivalent phreatic line and the one estimated from field observations are shown in Fig. 7*b*; similar comparison plots for each of the 10 participating cross-section locations are shown in Fig. A1 in Appendix A. For the cross-section at y = 138 m, Fig. 7*c* shows a comparison of bedrock profile estimated from the bedrock contours shown in Fig. 5 (1955 USGS quadrangle maps) with the one estimated from the bedrock contours shown in Fig. 2*a* (1940s Hamilton County 1 : 5000 survey map).

2-D continuum analyses

FLAC implements continuum-mechanics principles using the explicit finite difference formulation of the equation of motion. The geometry and location of the shear surface with the lowest FoS are obtained as a part of the FoS solution. The computed shear surface (geometry and location) is inferred from the shear strain-rate plot at the onset of numerical instability. The objective of these analyses is to compare the computed shear surface geometry and location with those observed and (or) estimated in the field. The pore pressure conditions used are those determined in the SSTAB2 analyses for FoS $\approx$ 1.

Figure 8*a* shows a typical FLAC model of a cross-section of the landfill at y = 138 m (Figs. 5 and 6), the associated leachate level, and the boundary conditions imposed; Fig. 8*b* shows the calculated shear surface location and geometry (steep path through the MSW and near level in the NS); Fig. 8*c* shows the computed elastic, yield in shear and tension state results (a graben-like feature appears). The shear strain-rate and elastic–plastic-tension state plots for each of the 10 participating cross-section locations are shown in Appendix A in Figs. A2 and A3, respectively. All of these results are encouraging as they compare favorably with the field observed shear surface geometry and the graben formation that formed on the day of the wasteslide. For each of the 10 cross-sections that participated in the wasteslide, the computed FoS results and comments on comparisons between computed and observed shear surface geometry and appearance of graben-like feature are included in Table 2. The FoS values are generally higher than those obtained using SSTAB2, and this is in accordance with the accepted trend that the simpler the solution procedure, the lower the computed FoS with all other variables being equal (this is in accord with the comment on FoS results using 2-D and 3-D slope stability analyses in Duncan 1996). In general, the computed location and geometry of the failure surface (steep head-scarp in the MSW and a near horizontal translational surface in the NS) and appearance of graben-like features compare well with the corresponding details of the landfill failure observed in the field.

3-D continuum analysis

FLAC3D is a 3-D counterpart of the FLAC 2-D continuum-mechanics based procedure described above. Figure 9 shows the FLAC3D model of the waste slope, the boundary condi-

Fig. 6. 2-D cross-sectional views of the landfill (Chugh and Stark 2003, reproduced with permission of Taylor & Francis NL, formerly Balkema).

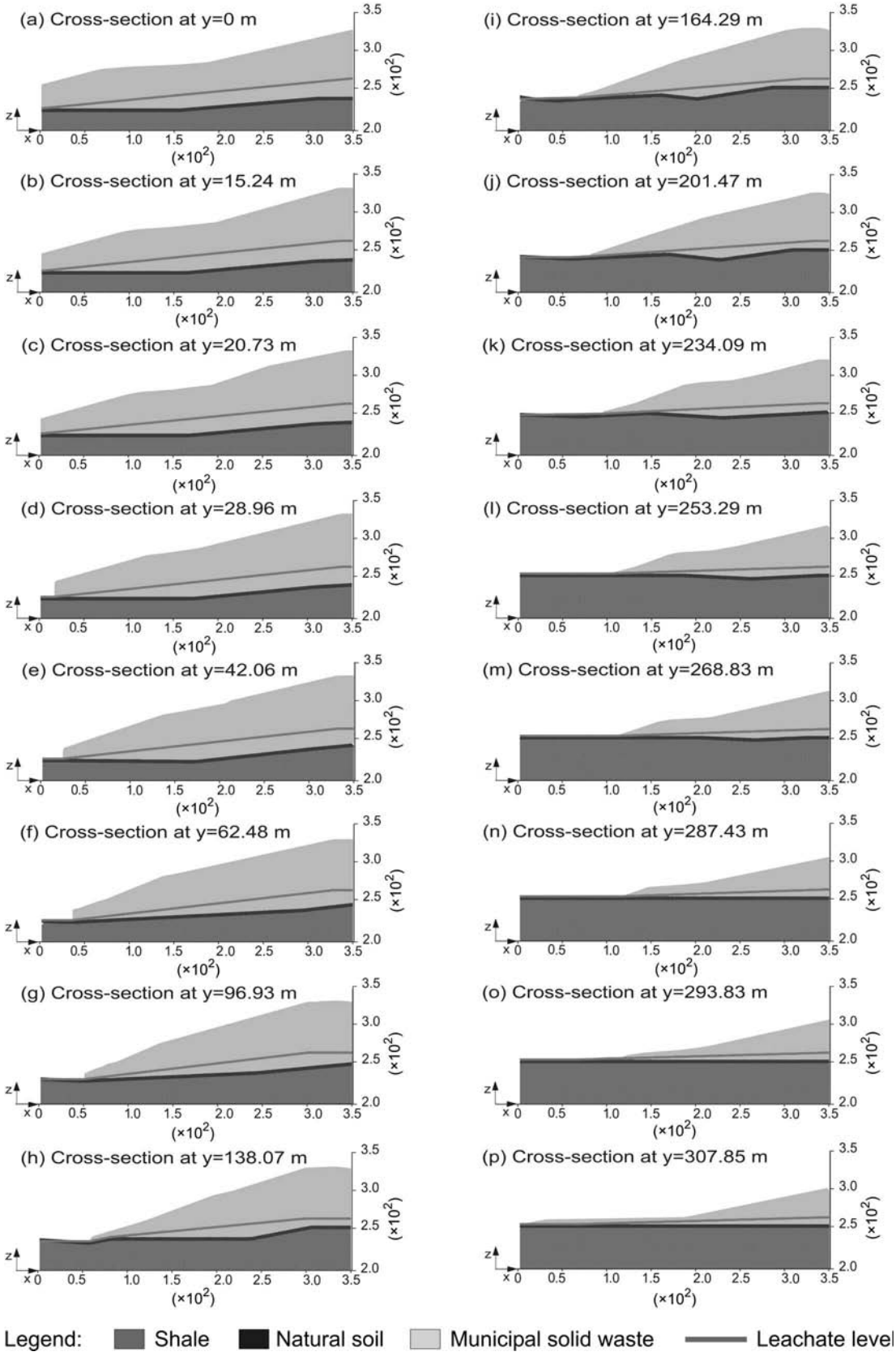

Table 1. Material properties for stability analyses of the municipal landfill slope failure near Cincinnati, Ohio, USA.

Material	Density, ρ (kg/m^3)	Material strength		Elastic constants	
		c (Pa)	ϕ (°)	Bulk modulus, K (Pa)	Shear modulus, G (Pa)
Municipal solid waste (MSW)	1040	4.0×10^4	35	1.1×10^8	5.0×10^7
Brown native soil (NS)	2010	0	12	3.0×10^8	3.0×10^7
Shale	2390	1.0×10^6	45	7.0×10^9	4.3×10^9
Interface in Fig. 11	NA	0	Varied during calculations from ϕ = 12° → ϕ = 5° in steps of 1°	Normal stiffness, 2.0×10^8 Pa/m	Shear stiffness, 6.3×10^6 Pa/m

Note: Unit weight γ (N/m^3) = ρ × 9.81; NA, not applicable.

Fig. 7. 2-D limit-equilibrium model of the landfill at $y \approx 138$ m for FoS calculations (typical).

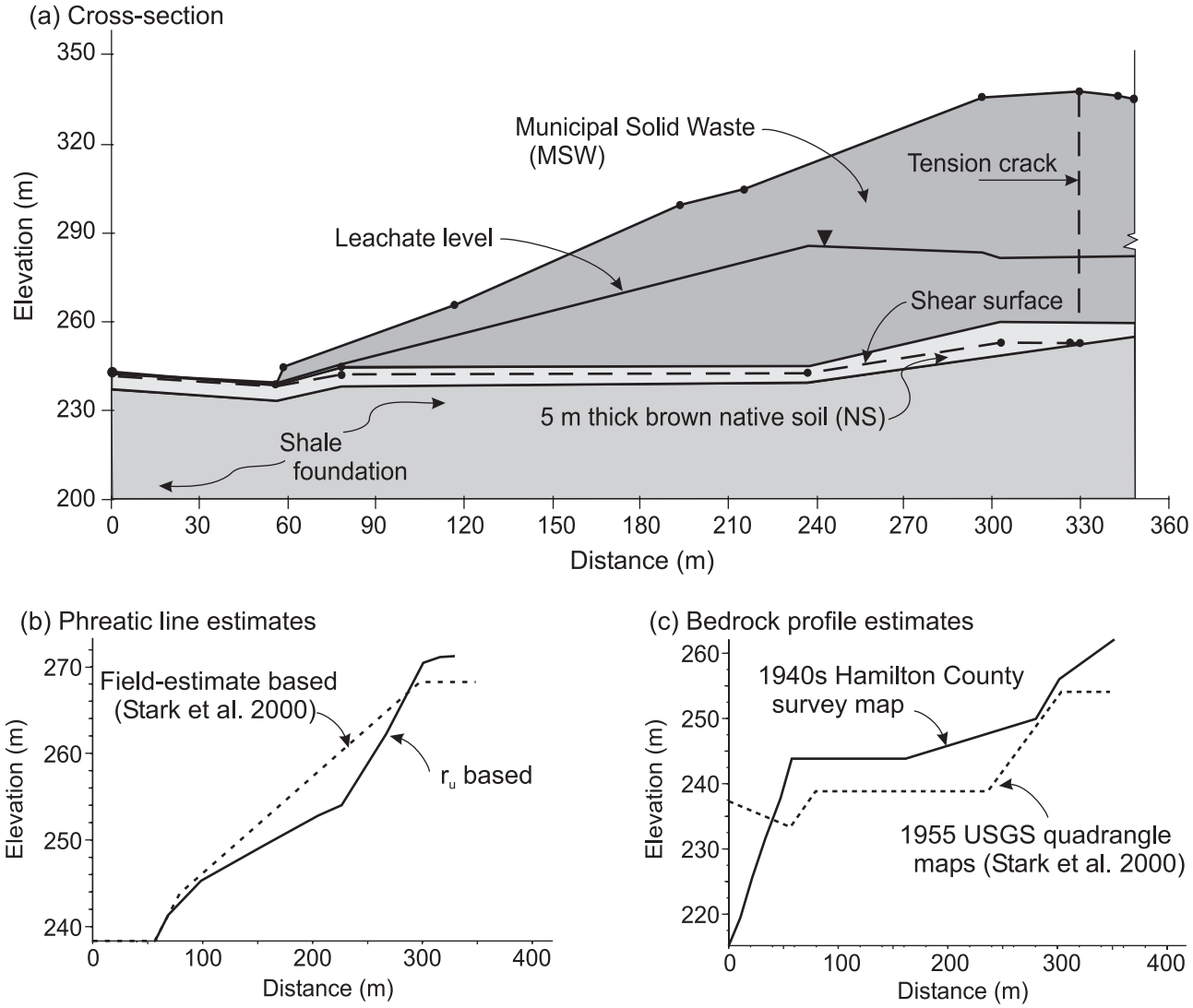

tions imposed, and the leachate surface (developed from the triangulation of the field estimated leachate levels in the landfill). The FLAC3D model for the landfill was created using the procedure presented in Chugh and Stark (2003). To avoid numerical problems, the excavation on the downslope side of the MSW toe was modeled as if it had MSW up to the elevation of the toe of the existing MSW. Thus the added artificial MSW overlies the added artificial 5 m thick NS on the shale foundation in the deep excavation area past the slope toe. The inclusion of this artificial MSW and the artificial NS in the deep excavation area is not expected to significantly (if at all) affect the FoS and shear surface results for the landfill under study as the two deposits (real MSW and real NS that failed and the MSW and NS added to avoid numerical problems) are linked via a connection that creates a discontinuity in the shear surface, i.e., the thickness

Table 2. Reanalyses results.

	2-D limit equilibrium solution: SSTAB2 results				2-D continuum solution: FLAC results					3-D continuum solution: FLAC3D results	Field data: Observed movements			
						Displacement* at $\phi = 6°$ (m)					Maximum displacement (m)			
						Toe		Head			Toe		Head	
Cross-section Id	H (m)	r_u for NS	FoS	δ (°)	FoS	u	w	u	w	FoS	u	w	u	w
Stn_0														
Stn_50														
Stn_68														
Stn_95	83.17	0.29	0.998	14.18	1.18	19	0	15	5					
Stn_138	89.67	0.22	0.990	14.99	1.21	4	0	0	0					
Stn_205	86.61	0.17	0.999	15.62	1.19	102	12	39	4					
Stn_318	84.39	0.19	0.995	16.76	1.14	186	23	21	3					
Stn_453	79.24	0.16	0.999	16.09	1.19	269	27	19	6	1.3	263	30	15	30
Stn_539	77.72	0.19	0.994	17.39	1.16	150	37	14	47					
Stn_661	67.47	0.30	0.989	14.80	1.24	0	0	0	0					
Stn_768	54.98	0.68	0.998	12.73	0.92	0	0	0	0					
Stn_831	41.63	0.62	0.994	22.84	1.15	0	0	0	0					
Stn_882	26.33	0.78	0.993	15.35	1.00	0	0	0	0					
Stn_943														
Stn_964														
Stn_1010														

Note: Formation of graben-like feature is interpreted from the plots of plastic yielding. Field data are based on field observations after the failure and contour maps.

*Values rounded to whole numbers.

of the real MSW and NS at the toe are essentially level and are merging into a relatively steep (downward) and thick head-deposit of the artificial MSW overlying a thin layer of artificial NS in the deep excavation; see Fig. 10*a*. Thus, the failure in the real MSW and real NS is expected to complete itself in the level stretch of the NS as it happened in the field.

The computed FoS for the waste slope is 1.30 as shown in Table 2. For a NS friction angle of 8°, the 3-D continuum FoS is 1.03. Figure 10 shows the details of the 3-D analysis (model, and plots of shear strain-rate and plastic state) at an *xz* plane (vertical section) located at $y = 138$ m (Figs. 5 and 6). In the 3-D model shown in Fig. 9*a*, the added MSW and NS in the excavation on the downslope side of the MSW are identified as mswt and nst, respectively. Once again, the shear surface geometry and graben-like features shown in Figs. 10*b* and 10*c*, respectively, agree well with the field observations. The shear strain-rate, and elastic–plastic-tension state plots for each of the 10 participating cross-section locations are shown in Appendix A in Figs. A4 and A5, respectively.

Displacement analyses

The computer program FLAC was also used to calculate displacements of the landfill at the 10 cross-sections located in the wasteslide shown in Fig. 5. The analysis procedure followed is: (*i*) model the NS layer as an interface with the interface properties shown in Table 1; (*ii*) impose an initial state of stress: $\sigma_{zz} = \rho g h$ and $\sigma_{xx} = \sigma_{yy} = K_0 \sigma_{zz}$ in the modeled materials; (*iii*) solve for equilibrium; (*iv*) release the $u = 0$ boundary condition for the MSW (at the vertical boundary located at the far end of the *x*-axis, Fig. 8*a*) and apply the *x*-reaction values as nodal forces along the freed boundary; (*v*) solve for equilibrium to verify step (*iv*); (*vi*) reduce the friction angle, ϕ, along the interface from 12° to 11°, solve for equilibrium within a maximum of 100 000 computational steps, and save the results; and (*vii*) repeat step (*vi*) by reducing the interface friction angle in steps of 1°. For each of the 10 cross-sections analyzed, the values of computed displacement at the toe and head of the slide mass corresponding to $\phi = 6°$ along the interface are shown in Table 2. For illustration, the displacement history at $y = 138$ m cross-section is shown in Fig. 11*a*, and positions of the displaced mass are shown in Figs. 11*b* and 11*c* for $\phi = 7°$ (initiation of noticeable movement) and for $\phi = 6°$ (final displaced location), respectively. Similar plots of displaced mass configuration for $\phi = 6°$ with elastic–plastic-tension state at each of the 10 participating cross-section locations are shown in Appendix A, Fig. A6. The abrupt movement of the landfill (calculated in going from $\phi = 7°$ to $\phi = 6°$) is interpreted to be indicative of a brittle (sudden) failure and agrees well with the rapid rate of failure observed in the field and the brittle behavior of the NS observed in laboratory testing.

The maximum computed horizontal (*x*) displacement occurs at the $y = 138$ m location. The maximum nonzero computed vertical (*z*) displacement occurs at the $y = 164$ m location. At the $y = 138$ m location, the *x*-displacement is 269 m, and the *z*-displacement is 27 m—the maximum *x*-displacement (at the toe) in the field is 263 m and the associated *z*-displacement is 30 m. At $y = 164$ m location, the *x*- and *z*-displacements (at the head)

Comparisons: Numerical results vs. field data – observation

Failure		Maximum displacements			
		Toe		Head	
Head scarp exit	Graben-like formation	*u*	*w*	*u*	*w*
good	yes				
poor	yes				
poor	yes				
good	yes				
good	yes	good (269/263)	good (27/30)	good (14/15)	poor (47/30)
good	yes				
good	no				
good	no				
poor	no				
good	no				

are 14 and 47 m, respectively—the corresponding field values are 15 and 30 m, respectively. These comparisons between the computed and observed displacements (except for the *z*-displacements at the head of the MSW) are considered to be good.

Site specific entities such as jointed bedrock; eruption of bedrock seepage through the compacted clay liner; discharge of steam from the cracks in the landfill; speed of the wasteslide and related dynamics of a moving mass; and ubiquitous-air are features of the actual failure but they are not considered in the numerical analyses. Their collective effect is taken to assert the following: the friction angle of 6° for the brown native soil, which yields the observed displacements, is considered reasonable (and in general, consistent with the residual friction angle of 10° to 12° from laboratory ring shear tests, Eid et al. 2000) because, in a gross sense, the value of 6° includes the effects of the above-mentioned site specific entities. Also, there will be some difference between the laboratory determined shear strength and the one calculated from numerical model studies for reasons such as: representative sample, field conditions, etc. amongst others. It is especially difficult to obtain a representative sample of a colluvial material.

Comments

(1) Analytical aspects of continuum models are all inclusive, i.e., limit-equilibrium models are subsets of continuum models. Limit-equilibrium models are restrictive in the aspects of a slope problem that can or cannot be included in an analysis; continuum models include virtually all aspects of mechanics of a slope problem in an analysis. In this sense, use of continuum models to reanalyze the landfill slope failure provides benefits over the limit-equilibrium models used in previous analyses of the landfill slope failure (Stark and Eid 1998; Stark et al. 2000).

(2) Slope stability analyses using the continuum approach are time consuming as compared to the use of limit-equilibrium analyses and this difference in time consumption increases with the dimensionality of the numerical model (2-D vs. 3-D). Displacement analyses using the continuum approach are even more time consuming. For the landfill slope failure analyses using FLAC, it took about 2 h for each of the 10 cross-sections for FoS calculations and about 3 days for each of the 10 cross-sections for displacement calculations; FoS calculations using FLAC3D took about 1 day. For comparison, FoS calculations using SSTAB2 took less than 1 min for each of the 10 cross-sections.

(3) The numerical analyses of the landfill slope failure using 2-D and 3-D continuum models provide means to compare the onset of failure (FoS $\approx$ 1), failure path (slip surface location and geometry), and final disposition of the slide mass (displaced position and configuration). This three parameter comparison (favorable) between the results from the continuum models of the landfill with the field observations of the landfill slope failure is considered to be an improvement over the single parameter match of FoS $\approx$ 1.

Fig. 8. 2-D continuum model of the landfill at $y \approx 138$ m for FoS calculations.

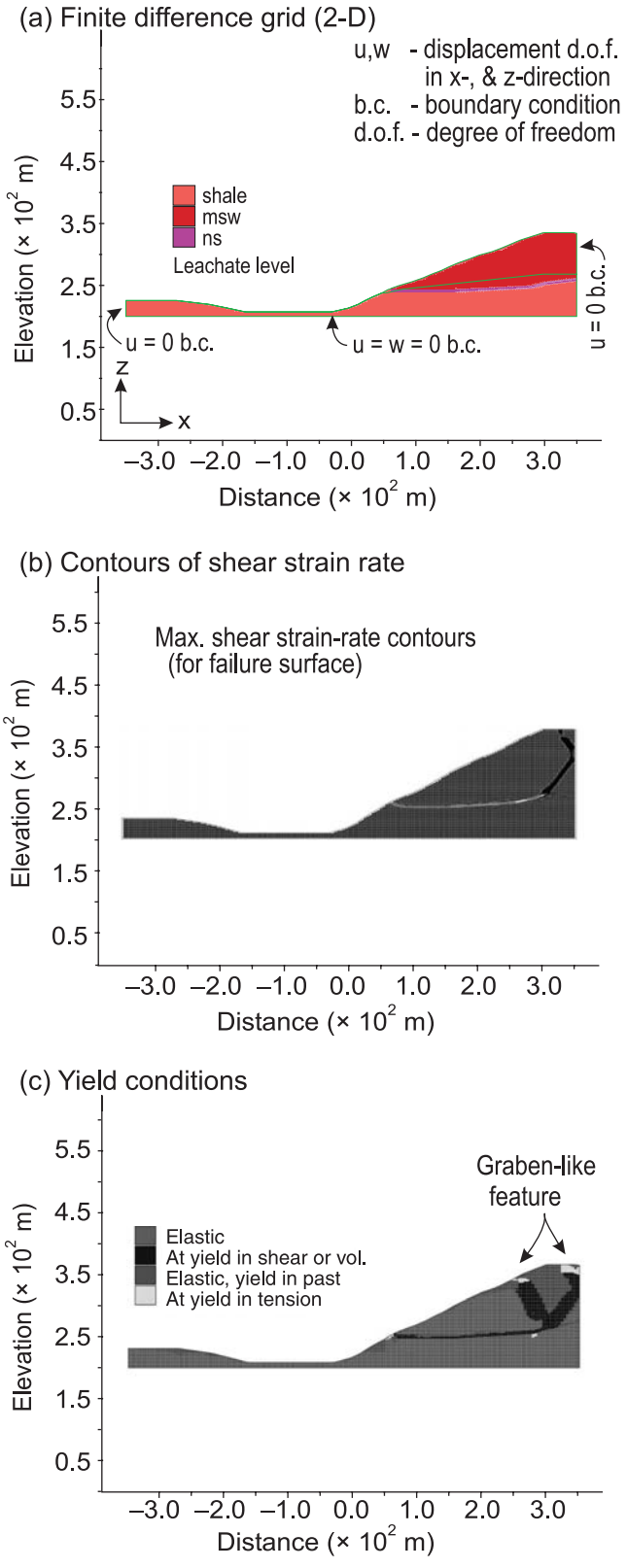

Fig. 9. 3-D continuum model for the landfill for FoS calculations. nst; artificial ns; ns, native soil; mswt, artificial msw; msw, municipal solid waste.

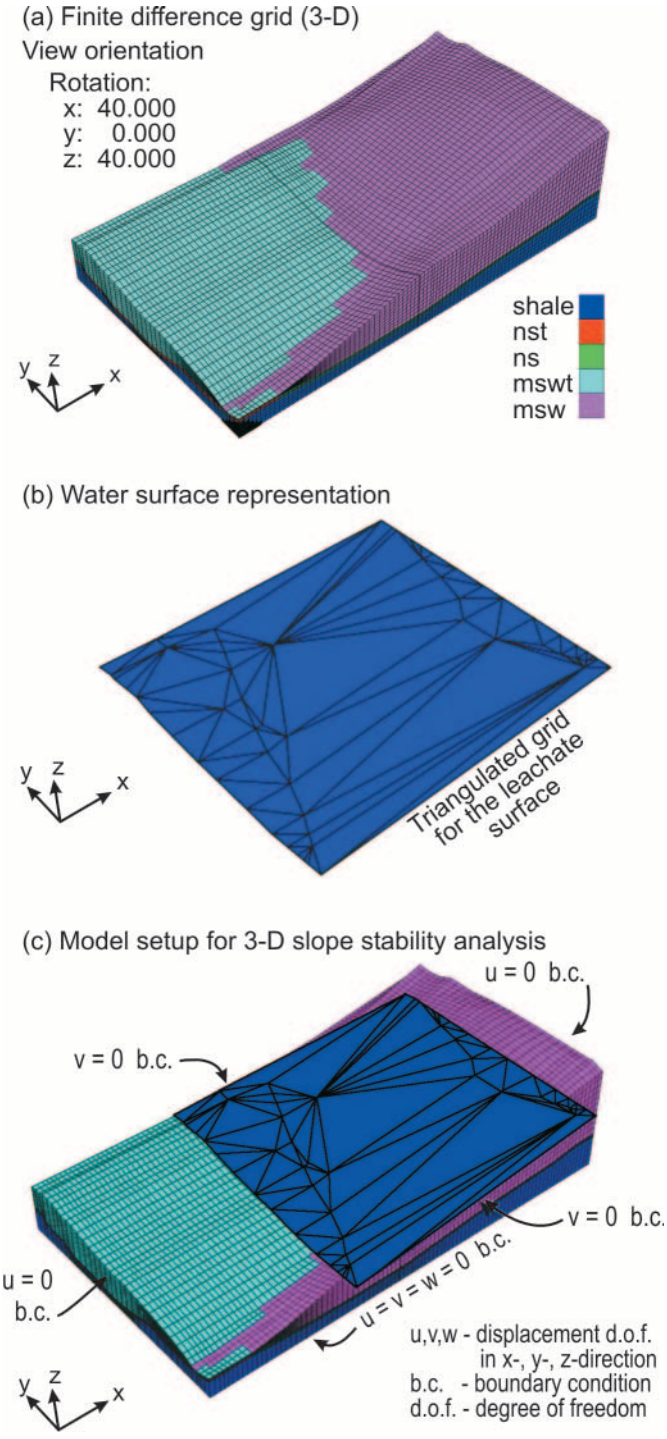

(4) The numerical analyses of the landfill slope failure were complicated because of: (*i*) scarcity of field data (such as spatial distribution of the waste placement, spreading and compaction, etc. from inception to the time of failure); (*ii*) available information based on analyses using models of varying complexities and details studying and (or) documenting likely cause(s) of the landfill slope

Fig. 10. 3-D slope stability results: at the cross-section location $y \approx 138$ m (typical).

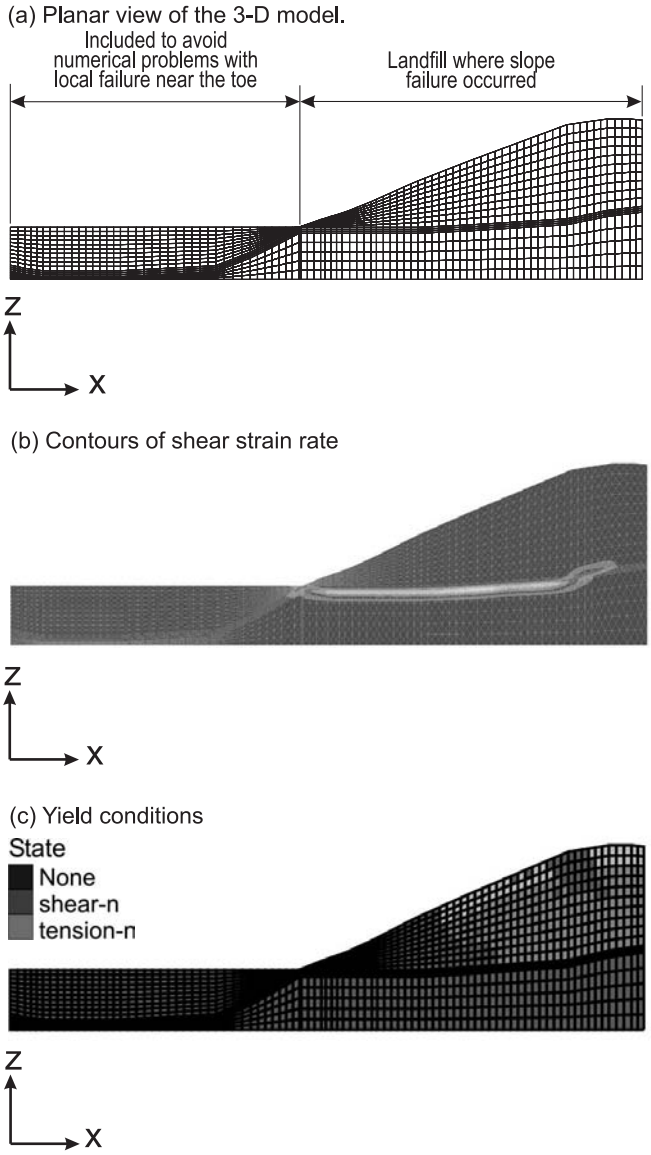

failure; and (*iii*) opinions formulated based on (*ii*). Different means (such as previously used data, different site maps, different failure hypotheses and models, assumptions regarding interface and interface properties values, etc.—not all of them necessarily consistent) were adopted to gain information deemed necessary for more complete analyses using the 2-D and 3-D continuum models of the landfill slope failure.

(5) Adaptation of the Brooker and Peck (1993) failure mechanism for the reanalysis of the landfill slope failure was motivated by the geometric similarities between the suggested and observed shear surfaces. Implementation of this failure mechanism in the SSTAB2 limit-equilibrium model required use of an artificial, liquid-filled tension crack to exert lateral earth pressure on the slide mass.

(6) In the limit-equilibrium based solution (SSTAB2 model), the failure surface is located entirely in the NS, and a ten-

Fig. 11. Computed displacement for the cross-section at $y \approx 138$ m (typical).

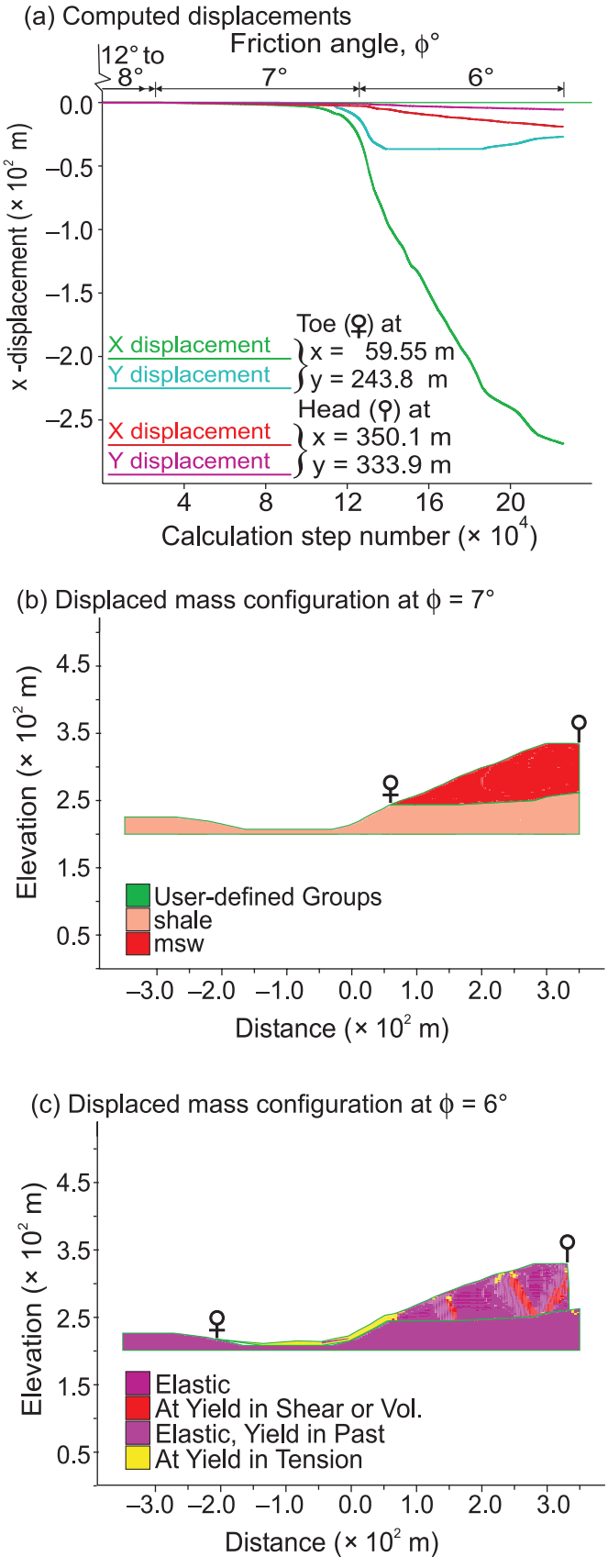

sion crack extends through the entire depth of the MSW. Thus, the shear strength of MSW did not influence the FoS results. The value of $K_0 = 0.43$ was estimated using the relation $K_0 = (1 - \sin \phi_{MSW})$. Applicability of this relation for MSW is questionable; however, the value of $K_0 = 0.43$ is well within the range of values (0.2 to 1.0) measured and reported in the past; see Kavazanjian (2006) for details and more recent findings on this and other aspects of waste mechanics. A numerical simulation of landfill placement and compaction, if known, would be an improvement over the analyses presented herein.

(7) The planar cross-sections used in the SSTAB2 analyses are based on initial estimates of bedrock elevation used and (or) presented in Stark and Eid (1998). However, in the FLAC and FLAC3D analyses, the bedrock contour map, Fig. 2*a*, was used. A reanalysis of the cross-section at $y = 138$ m with the bedrock contours of Fig. 2*a* using SSTAB2 results in FoS = 1.037 vs. 0.999 shown in Table 2.

(8) The FLAC results shown in Table 2 are based on r_u values calculated from SSTAB2 (for FoS ≈ 1). The leachate surface used in FLAC3D was developed from the field estimated leachate levels (Stark et al. 2000). This was done for convenience and (or) necessity using the information available during the analyses and to avoid duplication of work; however, necessary checks, using 2-D models, were exercised to ensure no substantial departure(s) from the information presented in this paper.

(9) Uniqueness of parameter values estimated from reanalyses of the landfill slope failure is neither intended nor implied; however, parameter values estimated and (or) used seem to be reasonable in view of the field observations, laboratory tests, and field performance of the landfill. It will be difficult, but may not be impossible, to find another consistent set of parameter values to make reasonable comparisons between the computed results and the actual failure at 10 cross-section locations for the three entities in 2-D and 3-D models: (*i*) onset of instability; (*ii*) geometry and location of failure surface; and (*iii*) maximum horizontal and vertical displacements at the toe and the head of the wasteslide. This has to be in addition to a reasonable comparison of graben-like formation(s) and break-up of the slide mass. No such attempts were made for the work included herein.

(10) Analytical and numerical details of the static slope stability and interface logic used in the continuum analyses reported in this paper are given in FLAC, and FLAC3D manuals; similarly, the analytical and numerical details of the static slope stability used in the limit-equilibrium analyses results included in this paper are given in the SSTAB2 manual. These details are not included here to conserve space.

Summary

The following observations are derived from the reanalysis of the landfill slope failure:

(1) There is a reasonable match between: (*i*) the computed slip surfaces and the observed failure surface in the field; (*ii*) the computed factor-of-safety (FoS ≈ 1) and actual slope failure; and (*iii*) the magnitudes of computed displacements and the observed movements in the field.

(2) At the onset of sliding failure of the landfill, the average friction angle for the brown native soil is about 8° from the 3-D continuum FoS analyses. In comparison, it is about 12° from the 2-D limit-equilibrium analyses. From the 2-D continuum analyses, it is less than 12°, since the FoS values are generally greater than 1. The general consensus that simpler calculations are generally conservative is supported by reanalyses of the landfill failure.

(3) The average field residual friction angle value of brown native soil could be as low as 6° as observed from a close comparison between the computed and observed displacements. The ring shear tests (in the laboratory) on the brown native soil gave a residual friction angle of about 10° to 12°. There are items such as generation of steam, energy of moving mass, and fragmentation of the slide mass, etc. that occur in the actual sliding mass but are not accounted for in the laboratory testing. This is taken to imply that the difference between the laboratory residual friction angle of 10° to 12° and the displacement-based calculated residual friction angle of 6° is within reasonable bounds. Displacement analyses of other slope failures (nonlandfills) suggest a residual friction angle of about 6° is possible (Stark and Eid 1997; Mesri and Shahien 2003; Chugh and Schuster 2003; Chugh and Stark 2005). However, additional displacement analyses of other slope failures are needed to verify the validity and (or) usefulness of a 6° residual friction angle as being representative of the final stage of a failed mass (independent of the material and the initial characteristics of the material).

(4) The landfill slide occurred abruptly after movement of the toe indicating a brittle failure. The laboratory ring shear data also show a brittle behavior of the brown native soil. These observations are in agreement with the displacement analysis that also shows an abrupt–brittle failure.

(5) The cause of initiation of the landfill failure can only be postulated since there were several detrimental activities occurring simultaneously, such as: (*i*) overfilling of the site; (*ii*) near vertical cut at the toe of the landfill; (*iii*) deep excavation on the downslope side of the landfill; (*iv*) blasting associated with rock excavation; and (*v*) start-up of the spring rainy season. These activities either individually or collectively facilitated the slope failure.

(6) Effective and efficient uses of 2-D and 3-D continuum models to study onset of instability, failure path geometry and location, and displacements associated with slope failures are within the reach of practicing engineers equipped with personal computers and commercially available continuum-mechanics-based computer programs. However, some new learning and experience are needed to make a transition from the use of limit-equilibrium-based slope stability analysis procedures to the use of continuum-mechanics-based analysis procedures with confidence and awareness.

Acknowledgement

The authors would like to express their sincere thanks to Professor Edward Kavazanjian, Jr. for his helpful comments on the initial version of the paper. Revisions to the paper were facilitated by study of an advance copy of his Keynote Paper in the June 2006 Geoshanghai International Conference.

References

Baum, R.L., and Johnson, A.M. 1996. Overview of landslide problems, research and mitigation, Cincinnati, Ohio, area. United States Geological Survey Bulletin 2059-A. United States Government Printing Office, Washington, D.C.

Brooker, E.W., and Peck, R.B. 1993. Rational design treatment of slides in overconsolidated clays and clay shales. Canadian Geotechnical Journal, **30**: 526–544.

Chugh, A.K. 1992. User information manual for slope stability analysis program SSTAB2. United States Bureau of Reclamation, Denver, Colo.

Chugh, A.K., and Schuster, R.L. 2003. Numerical assessment of Locke Island landslide, Columbia River Valley, Washington State, USA. *In* Proceedings of the 12th Panamerican Conference on Soil Mechanics and Geotechnical Engineering, Cambridge, Mass., 22–26 June 2003. Verlag Glückauf, Essen, Germany. pp. 2489–2496.

Chugh, A.K., and Stark, T.D. 2003. An automated procedure for 3-dimensional grid generation. *In* Proceedings of the 3rd International FLAC Symposium, Sudbury, Ontario, 21–24 October 2003. A.A. Balkema, Lisse, The Netherlands. pp. 9–15.

Chugh, A.K., and Stark, T.D. 2005. Displacement analysis of a landslide. *In* Proceedings of the 11th International Conference and Field Trip on Landslides, Norway, 1–10 September 2005. Taylor & Francis Group, London. pp. 73–81.

Duncan, J.M. 1996. State of the art: Limit equilibrium and finite-element analysis of slopes. Journal of Geotechnical Engineering, **122**: 577–596.

Duncan, J.M., and Wright, S.G. 2005. Soil strength and slope stability. John Wiley & Sons, Inc., N.J.

Eid, H.T., Stark, T.D., Evans, W.D., and Sherry, P.E. 2000. Municipal solid waste slope failure. I: Waste and foundation soil properties. Journal of Geotechnical and Geoenvironmental Engineering, **126**: 397–407.

Hungr, O. 1988. User's manual: CLARA 2.31, Slope stability analysis in two or three dimensions for IBM compatible microcomputers. Oldrich Hungr Geotechnical Research, Inc., Vancouver, B.C.

Itasca Consulting Group. 2000. FLAC – Fast Lagrangian Analysis of Continua. Itasca Consulting Group, Minneapolis, Minn.

Itasca Consulting Group. 2002. FLAC3D – Fast Lagrangian analysis of continua in three dimensions. Itasca Consulting Group, Minneapolis, Minn.

Kavazanjian, E., Jr. 2006. Waste mechanics: recent findings and unanswered questions. *In* Advances in unsaturated soil, seepage, and environmental geotechnics. ASCE Geotechnical Special Publication No. 148, pp. 34–54.

Kavazanjian, E., Beech, J.F., and Matasović, N. 2001. Discussion: municipal solid waste slope failure. I: Waste and foundation soil properties. Journal of Geotechnical and Geoenvironmental Engineering, **127**: 812–815.

Mesri, G., and Shahien, M. 2003. Residual strength mobilized in first-time slope failures. Journal of Geotechnical and Geoenvironmental Engineering, **129**: 12–31.

Spencer, E. 1967. A method of analysis of the stability of embankments assuming parallel interslice forces. Géotechnique, **17**: 11–26.

Stark, T.D., and Eid, H.T. 1997. Slope stability analyses in stiff fissured clays. Journal of Geotechnical and Geoenvironmental Engineering, **123**: 335–343.

Stark, T.D., and Eid, H.T. 1998. Performance of three-dimensional slope stability methods in practice. Journal of Geotechnical and Geoenvironmental Engineering, **124**: 1049–1060.

Stark, T.D., Eid, H.T., Evans, W.D., and Sherry, P.E. 2000. Municipal solid waste slope failure. II: Stability analyses. Journal of Geotechnical and Geoenvironmental Engineering, **126**: 408–419.

Appendix A

In this appendix, all results are presented in figures; references to these figures are made in the text of the paper. No additional comments are deemed necessary.

Fig. A1. Comparison of calculated equivalent phreatic line and the estimated phreatic line from field observations.

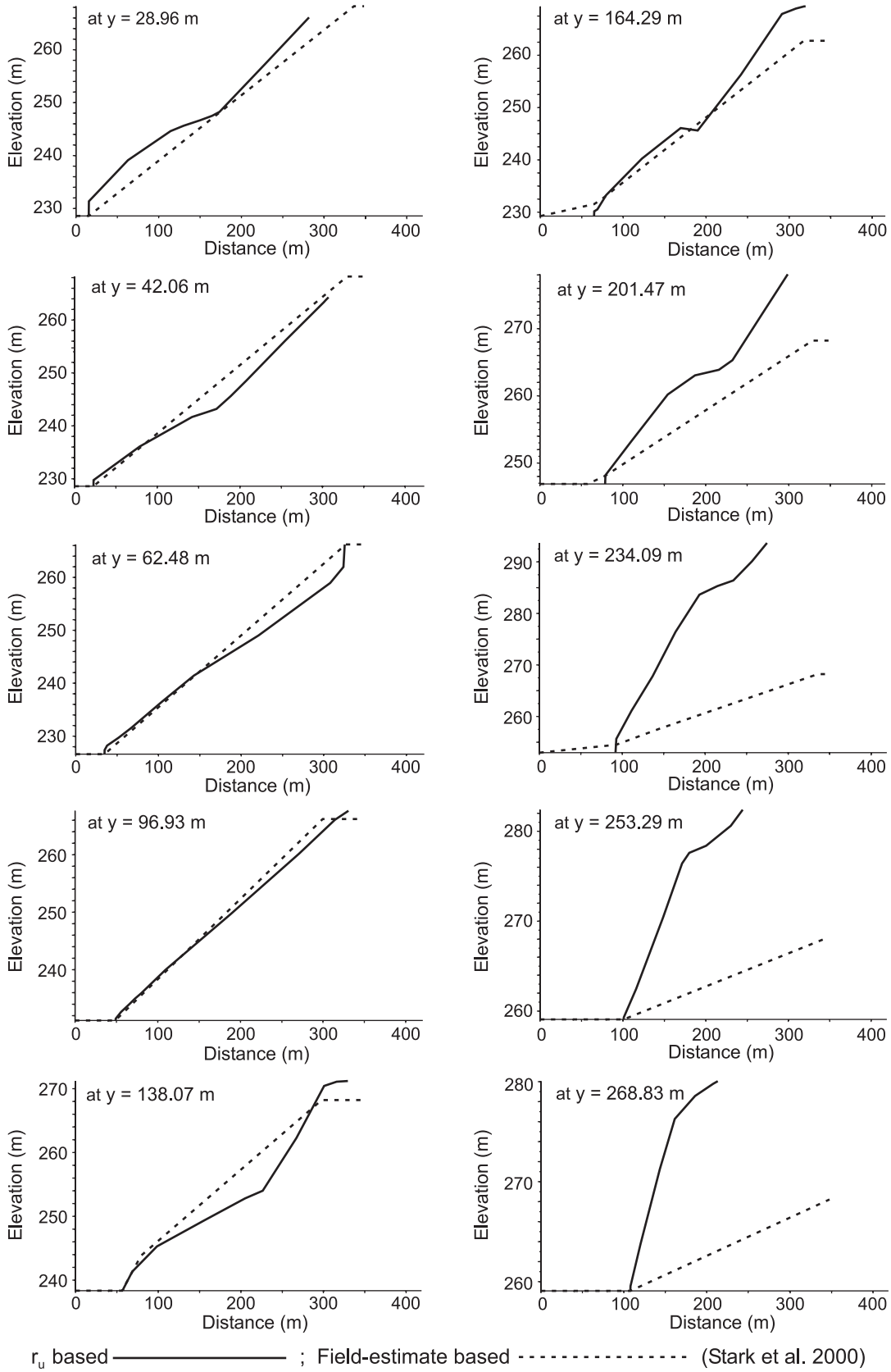

Fig. A2. 2-D continuum model results of shear strain-rate used to interpret the geometry and location of failure surfaces.

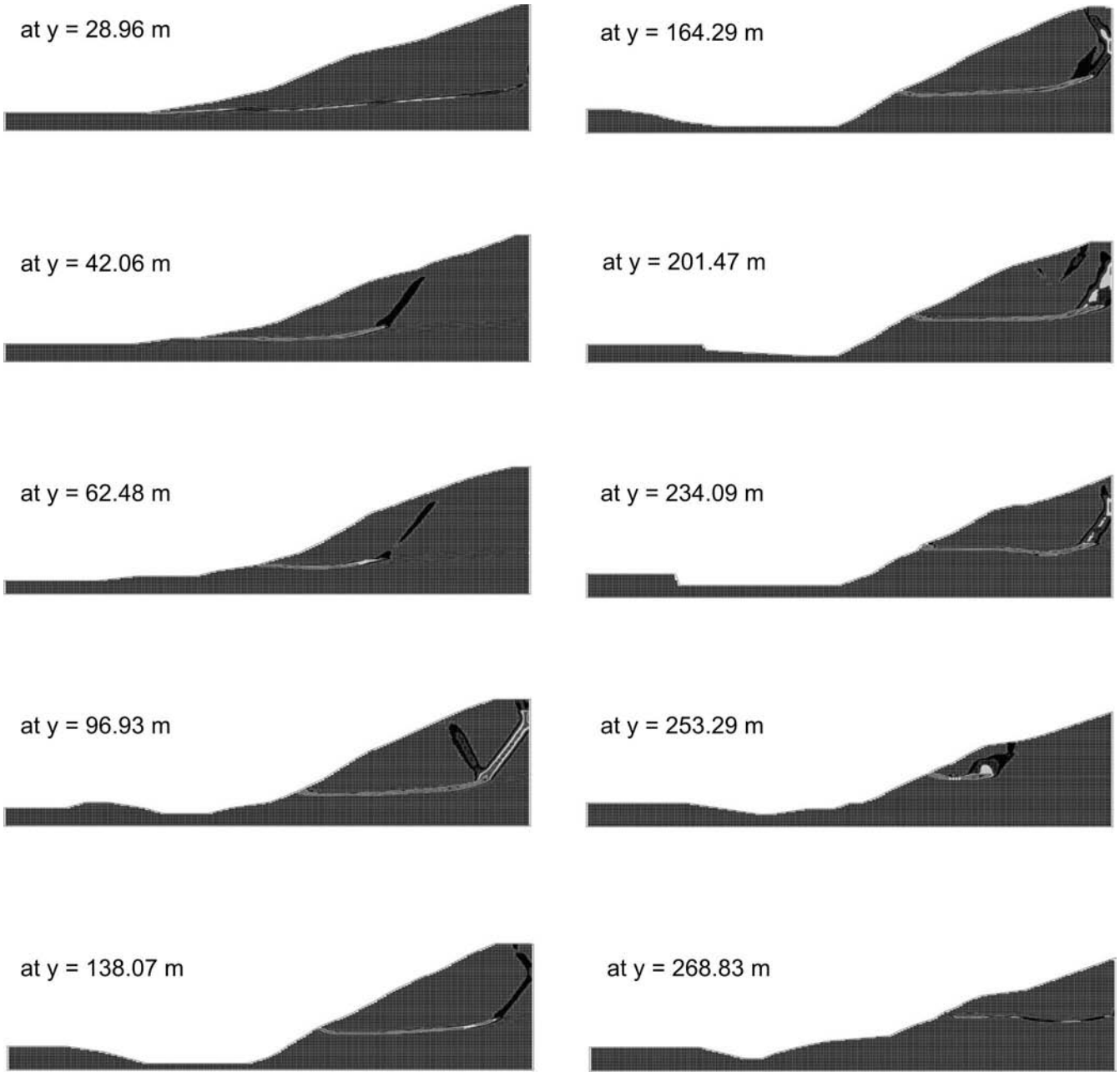

Fig. A3. 2-D continuum model results of elastic–plastic-tension state used to interpret failure patterns.

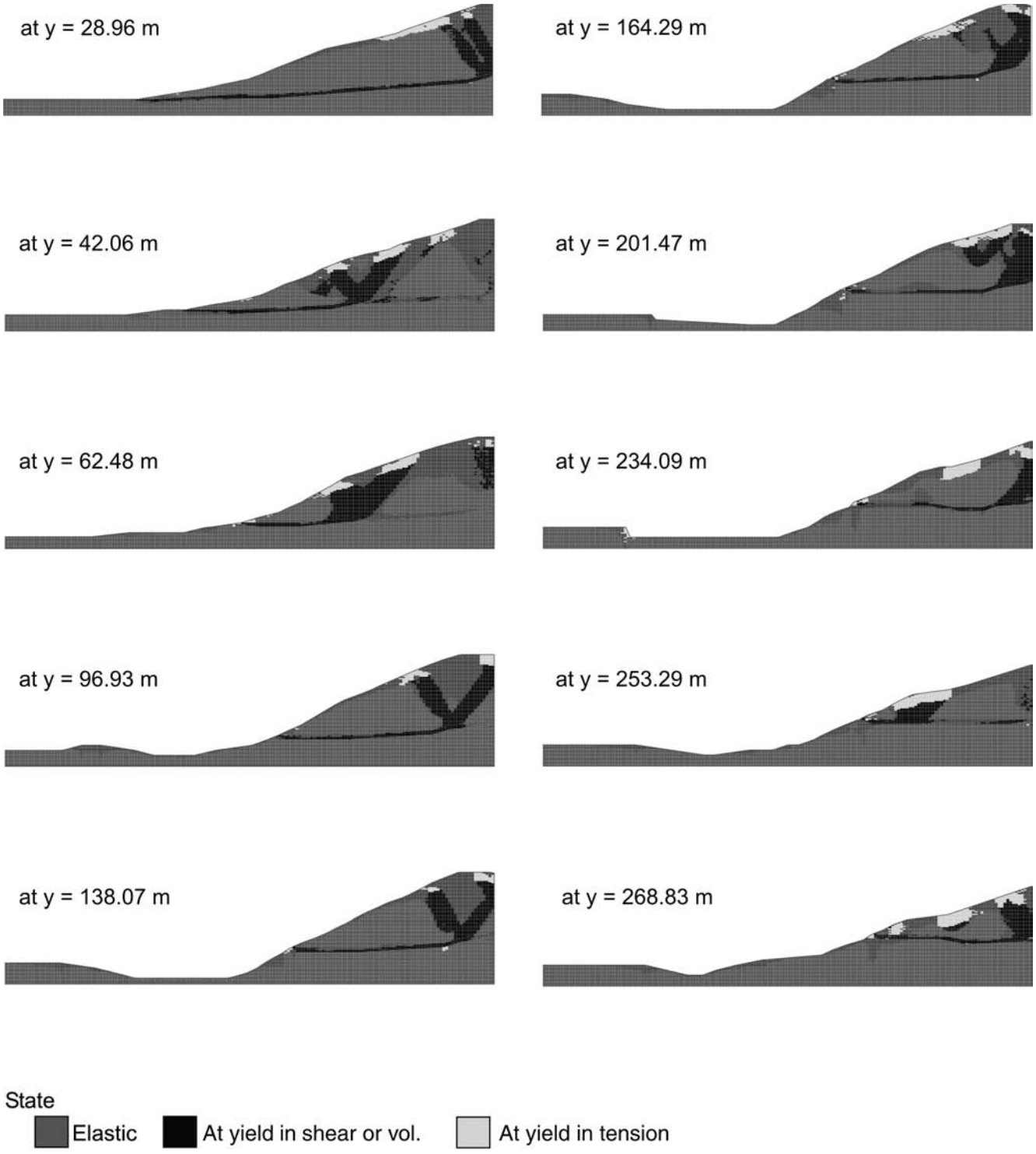

Fig. A4. 3-D continuum model results of shear strain-rate used to interpret the geometry and location of failure surfaces.

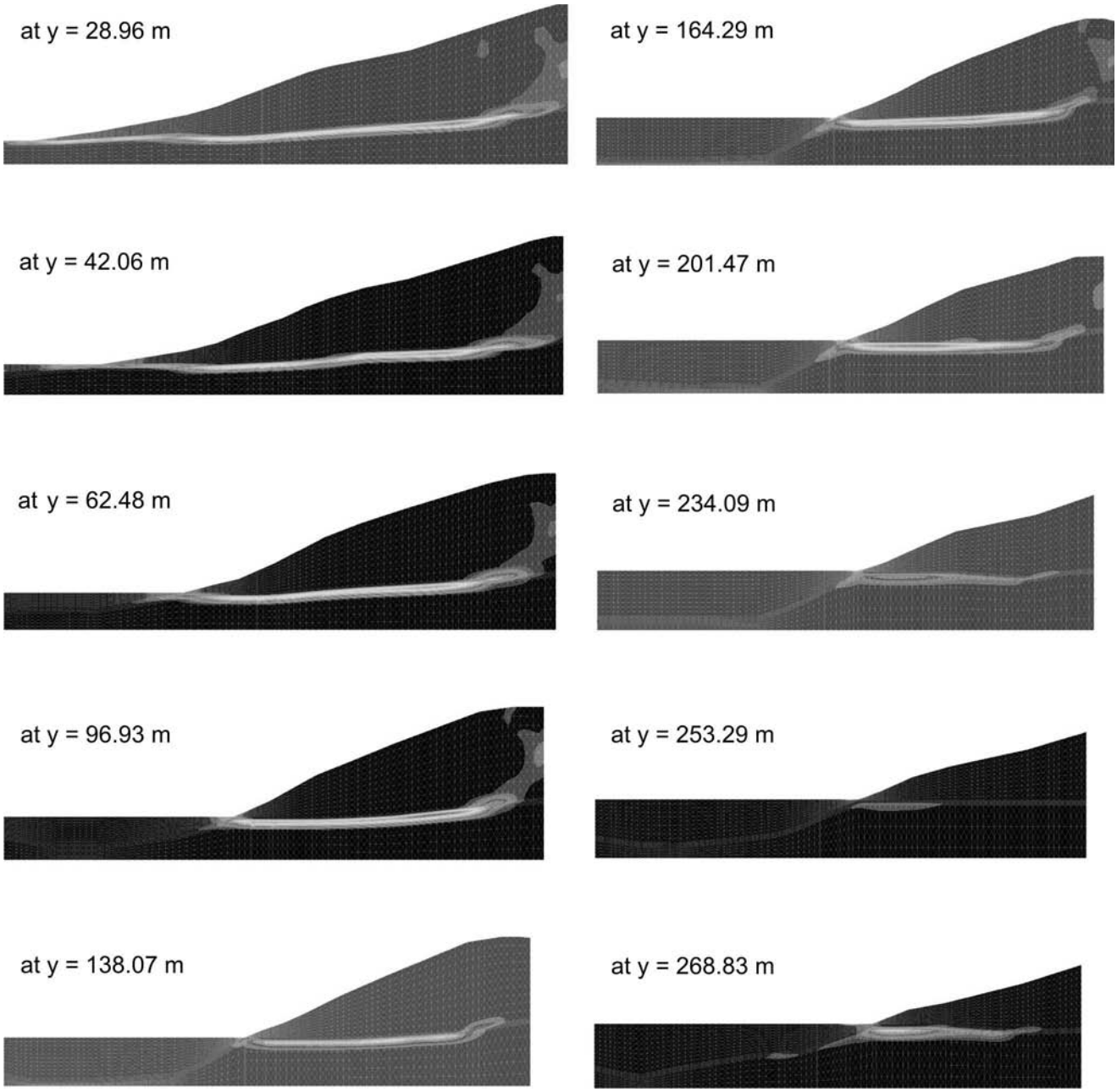

Fig. A5. 3-D continuum model results of elastic–plastic-tension state used to interpret failure patterns.

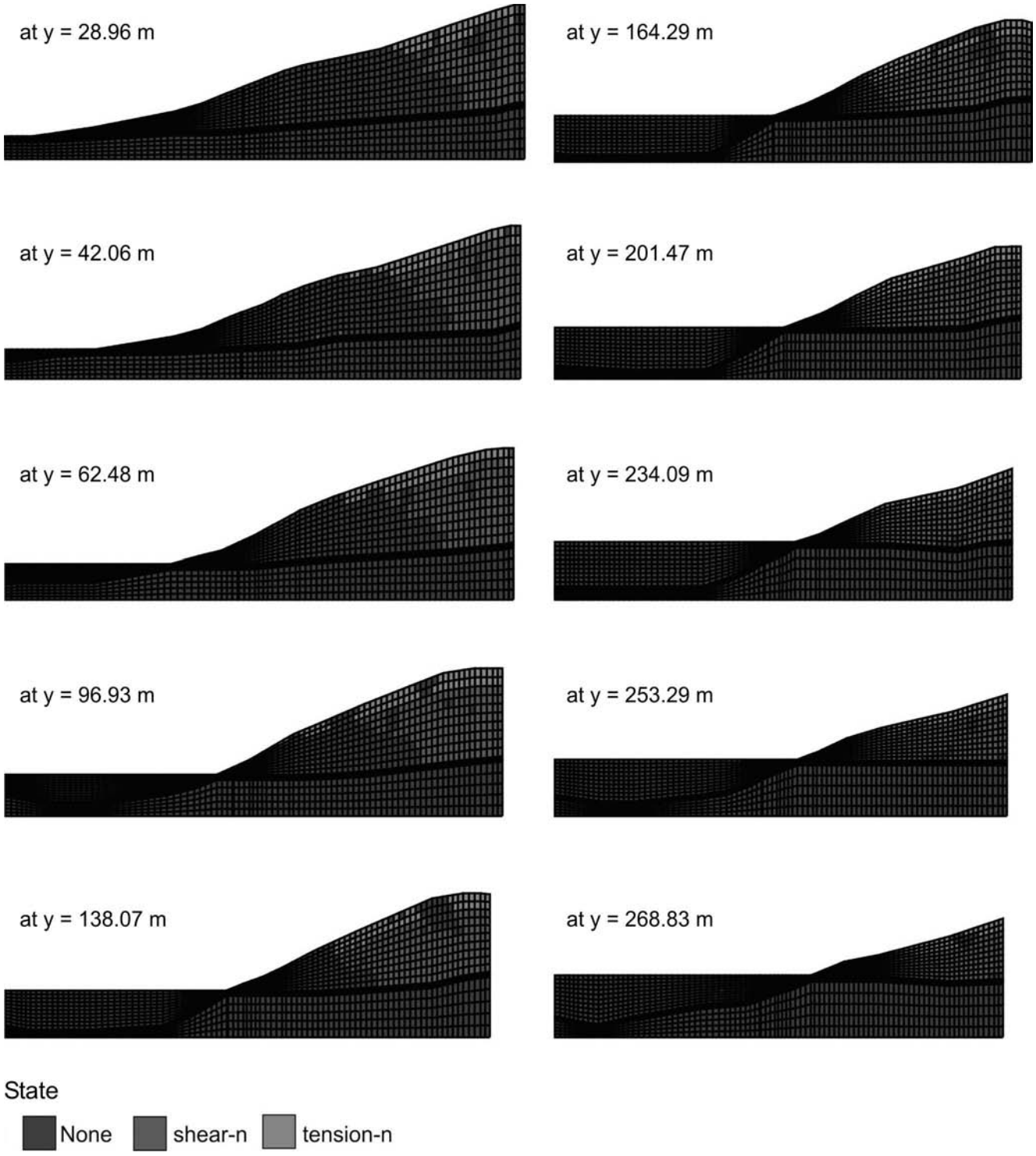

Fig. A6. 2-D continuum model results of displaced mass configuration at $\phi = 6°$.